Hindawi
Advances in Civil Engineering
Volume 2022, Article ID 3573608, 19 pages
https://doi.org/10.1155/2022/3573608

Research Article

Hyperelastic Geometrically Nonlinear Inverse 3D-FEM Truss Analyses Based on VaReS

Klaus Bernd Sautter and Kai-Uwe Bletzinger

Chair of Structural Analysis, Technical University of Munich, Arcisstr 21, Munich 80333, Germany

Correspondence should be addressed to Klaus Bernd Sautter; klaus.sautter@tum.de

Received 5 July 2022; Revised 28 September 2022; Accepted 30 September 2022; Published 1 December 2022

Academic Editor: Michael Yam

Direct usage of construction plans as input for structural analyses assumes the reference configuration to match the engineering drawings. However, the built construction is typically supposed to match the construction plans after its successful erection. In that state, the structure is usually already subjected to self-weight and maybe other loadings. Consequently, an analysis approach is necessary to find the unknown reference configuration for a given, desired deformed structural shape. The standard static problem needs to be reformulated with the reference coordinates being the unknown variables. This work describes the necessary steps for geometrically and materially nonlinear truss elements based on the variation of reference strategy (VaReS) and gives a highly detailed description of all resultant system derivatives. Arbitrary hyperelastic material laws can be applied of which this work introduces the St. Venant-Kirchhoff, the Neo-Hookean, and the Ogden law. Additionally, the self-weight load case is considered, increasing the problem's nonlinearity. Finally, two- and three-dimensional structural problems are presented to show the solution capabilities, ranging from simple 3-bar systems to larger framework bridges. While all necessary vectors and matrices are discussed and presented in great detail, a publicly available GitHub repository makes the code freely accessible as Python code.

1. Introduction

Direct usage of construction plans as input for structural analyses assumes the reference configuration to match the engineering drawings. However, the built construction is typically supposed to match the construction plans after its successful erection. In that state, the structure is usually already subjected to self-weight and maybe other loadings. Consequently, an analysis approach is necessary to find the unknown reference configuration for a given, desired deformed structural shape.

In conventional structural analysis, a given configuration is typically loaded and subsequently simulated, resulting in deformations and stress states. Often, this analysis is unsuitable, and an "inverse" analysis must be performed. Especially for lightweight membrane or cable net constructions, the internal stress state is predefined, and a corresponding equilibrium shape is searched. Moreover, the desired deformed shape is given for specific structures, and an unknown reference configuration needs to be found. Standard structural analysis is not applicable in these cases, and other solution methods must be utilized. Overall, the finite element method (FEM) has proven to be one of the most effective approaches and will also be the basis for the presented method.

Several approaches have been developed to find an equilibrium shape for a given stress state (including external forces). Exploiting proven dynamic simulation strategies the dynamic relaxation approach [1–3] creates a dynamic problem, based on the underlying static problem. Similar to an explicit dynamic simulation, no stiffness matrices are necessary, and a simple node-based solution loop can be used to calculate the artificially damped structure until an equilibrium shape has been found.

Directly working with the static problem [4–6] has developed the force density method, whose first successful and practical application can be admired in Munich in the form of the roof of the Olympic Stadium [7]. This approach

assembles nodal force equilibrium equations and keeps the ratio of internal force and element length constant, creating a linear system of equations out of a normally nonlinear system. Reference [8] proposes the SGC (statically geometrically coupled) method as an extension to the force density, considering geometrical specifications. The updated reference strategy (URS), developed by [9, 10], is a generalization of the force density method. It is derived from continuum mechanics of elastic bodies and closely follows the FEM approach, allowing its application to any structure. The URS is not restricted to one-dimensional structures compared to the force density method. Based on the URS, form-finding for hybrid structures is discussed in [11], and a description of the whole engineering design cycle is given in [12]. Further approaches are available, such as analyses based on graphic statics [13–15] and constrained form-finding using automated differentiation [16].

In contrast to the discussed form-finding strategies, [17, 18] developed the variation of reference strategy (VaReS), inspired by [19]. It is further discussed in [20] and later applied to the concept of isogeometric B-Rep analysis (IBRA) in [21]. VaReS is typically employed to analyze suitable cutting patterns for prestressed membrane structures. It is based on a change of the system unknowns, called the "concept of inverse mechanics" by [17], originating from [22, 23]. A similar strategy is followed by [24] to analyze sheet metal forming. Here, the reference (undeformed configuration) represents the unknown variables instead of the structural displacements. While standard structural analyses typically result in the deformed spatial configuration with a known material configuration, the inverse analysis uses an initially given spatial (deformed) configuration to solve for a suitable unknown material (reference, undeformed) configuration. Figure 1 graphically explains this concept. The idea of "inverse engineering" was already discussed in [25–27] and successfully applied to cutting pattern generations for isotropic materials in the linear and moderately nonlinear regime.

While a very short introduction to a two-dimensional truss element can be found in [17], this work takes up the "concept of inverse mechanics" to find unknown reference geometries for three-dimensional truss structures. With the help of the presented approach, the engineer can determine the necessary reference construction so that the desired final aim geometry is obtained for a given load state. To allow a wide range of application cases, the base equations are geometrically and materially nonlinear. Arbitrary nonlinear hyperelastic material laws can be used within this workflow, of which the St. Venant-Kirchhoff law, the Neo-Hookean law, and the Ogden law are introduced herein. Consequently, we add the effects of self-weight inclusion on the solution procedure and present various test cases to prove the effectiveness and simulation capabilities of the proposed approach. Particular focus is put on the extensively detailed presentation of all necessary derivatives and every step towards the final solution. Additionally, all system matrices, examples, and a simulation framework are made publicly accessible via a GitHub repository [28] as Python code.

The work is thematically structured as follows:

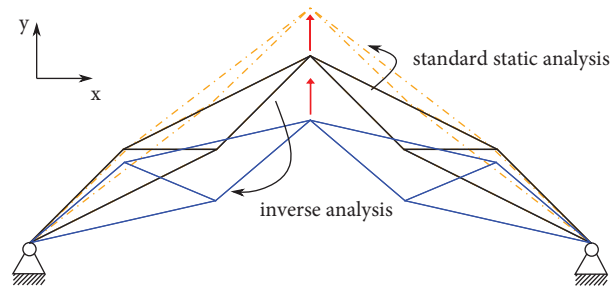

Figure 1: A standard static analysis calculates the deformation of a given reference configuration, and the displacements are the unknown variables. The inverse analysis is used to determine the unknown reference configuration for a given deformed state.

(i) Section 2 introduces the general truss formulation, including material law and other assumptions. This section is necessary to later follow up with the detailed investigation of all its derivatives.

Subsection 2.1 formulates the nonlinear truss formulation, presenting the internal element forces, based on nonlinear stress and strain measures

Subsection 2.2 discusses simplifications for linear strain and deformation regimes

(ii) Section 3 subsequently formulates the global problem and the resulting system of equations
Subsection 3.1 discusses the standard global force equilibrium in the reference configuration.
Subsection 3.2 afterwards derives the inverse problem, reformulating the force equilibrium from the previous subsection.

(ii) Section 3 subsequently formulates the global problem and the resulting system of equations
Subsection 3.1 discusses the standard global force equilibrium in the reference configuration.
Subsection 3.2 afterwards derives the inverse problem, reformulating the force equilibrium from the previous subsection.
Subsection 3.1 discusses the standard global force equilibrium in the reference configuration.
Subsection 3.2 afterwards derives the inverse problem, reformulating the force equilibrium from the previous subsection.

(iii) Section 4 follows up with a variety of different test cases. Two- and three-dimensional truss structures are discussed. Investigations of convergence rates are included for selected examples.

(iv) Section 5 concludes this work.

2. Truss Formulation

The truss element in this work is described by two nodes connected by a linear, straight line, as depicted in Figure 2. It

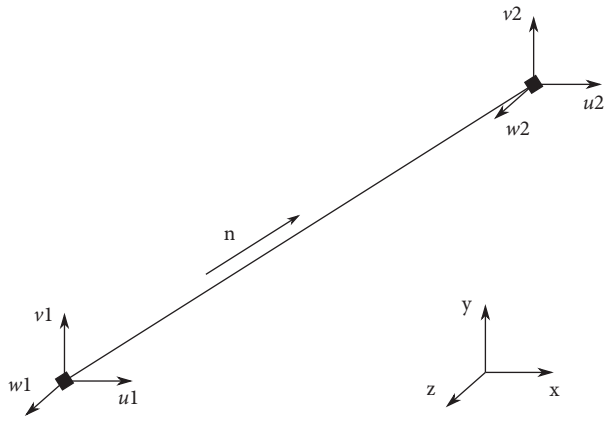

Figure 2: Linear truss element with nodal degrees of freedom.

carries only normal forces and keeps a constant cross section A by neglecting the Poisson's effect.

Each node has three translational degrees of freedom (dofs), which are assembled for every element in the displacement vector $\mathbf{u}_e$, respectively,

$$\mathbf{u}_e = [\, \mathbf{u}_{e,1} \;\; \mathbf{u}_{e,2} \,] = [\, u_1 \;\; v_1 \;\; w_1 \;\; u_2 \;\; v_2 \;\; w_2 \,]. \tag{1}$$

Additionally, we introduce the discrete reference nodal coordinates per element $\mathbf{X}_e$, as well as the discrete actual nodal coordinates per element $\mathbf{x}_e$,

$$\mathbf{X}_e = [\, X_1 \;\; Y_1 \;\; Z_1 \;\; X_2 \;\; Y_2 \;\; Z_2 \,], \tag{2}$$

$$\mathbf{x}_e = [\, x_1 \;\; y_1 \;\; z_1 \;\; x_2 \;\; y_2 \;\; z_2 \,]. \tag{3}$$

Using the reference coordinate differences dX, dY, dZ, the reference length L can be calculated as

$$\begin{aligned} L &= \sqrt{dX^2 + dY^2 + dZ^2}, \\ dX &= X_2 - X_1, \\ dY &= Y_2 - Y_1, \\ dZ &= Z_2 - Z_1. \end{aligned} \tag{4}$$

The same operation holds for the calculation of the deformed element length l

$$\begin{aligned} l &= \sqrt{dx^2 + dy^2 + dz^2}, \\ dx &= x_2 - x_1, \\ dy &= y_2 - y_1, \\ dz &= z_2 - z_1. \end{aligned} \tag{5}$$

2.1. Large Deformations—Nonlinear Truss Formulation. Following the well-known FEM approach, the total virtual work δW is expressed by the virtual internal work δW_{int} and the virtual external work δW_{ext}

$$\delta W = \delta W_{int} - \delta W_{ext} = 0. \tag{6}$$

This will result in a stiffness matrix and a force vector to solve the static problem. We will discuss the derivation of the global three-dimensional stiffness matrix in the following, leading to the global problem formulation. The virtual internal work is formulated by integrating over the reference volume $V = A\,L$ as the product of the reference area A and the reference length L

$$\begin{aligned} \delta W_{\text{int}} &= \int_V S\delta\varepsilon \, \mathrm{d}V = ALS\delta\varepsilon \\ &= ALS \frac{\partial \varepsilon}{\partial \mathbf{u}_e} \delta \mathbf{u}_e. \end{aligned} \tag{7}$$

To allow for the analysis of arbitrarily large deformations and correctly considering rigid body rotations, nonlinear strain and stress measurements are applied. While S represents the 1D 2 nd Piola-Kirchhoff stress, the work-conjugated 1D Green-Lagrange strain is described by ε as follows:

$$\varepsilon = \frac{1}{2} \frac{l^2 - L^2}{L^2}. \tag{8}$$

Based on the chosen material law and its associated Helmholtz free-energy function Ψ, the 2 nd Piola-Kirchhoff stress and the respective material tangent modulus $\mathbb{C}$ can be evaluated as follows:

$$\begin{aligned} S &= \frac{\partial \Psi}{\partial \varepsilon}, \\ \mathbb{C} &= \frac{\partial S}{\partial \varepsilon} = \frac{\partial^2 \Psi}{\partial \varepsilon^2}. \end{aligned} \tag{9}$$

S and $\mathbb{C}$ are exemplarily given for three different hyperelastic material laws in the following. They can be plugged into the derivations of this work to analyze and simulate different deformation behaviors.

(1) *St. Venant-Kirchhoff*
$S = E\,\varepsilon$
$\mathbb{C} = E$

(2) *Neo-Hookean*
$S = E\varepsilon/(2\varepsilon + 1)$
$\mathbb{C} = E\varepsilon/(2\varepsilon + 1)$

(3) *Ogden* β_1, β_2 are specific Ogden parameters and need to be chosen appropriately.
$S = (E/\beta_1 - \beta_2)\;((2\varepsilon + 1)^{(\beta_1/2)-1} - (2\varepsilon + 1)^{(\beta_2/2)-1})$
$\mathbb{C} = (E/\beta_1 - \beta_2) \qquad ((\beta_1 - 2)(2\varepsilon + 1)^{(\beta_1/2)-2} - (\beta_2 - 2)(2\varepsilon + 1)^{(\beta_2/2)-2})$

Specifically, the Ogden law is of major importance as it can be easily transformed into other constitutive laws, such as the St. Venant-Kirchhoff law ($\beta_1 = 4, \beta_2 = 2$) and the Neo-Hookean law ($\beta_1 = 2, \beta_2 = 0$) [29, 30]. Special attention needs to be paid when dealing with large compressive strains. As discussed in [29], the St. Venant-Kirchhoff law is not appropriate for this case anymore, and other material laws are recommended.

Finally, the internal element forces $\mathbf{F}_{int,e}$ are derived from (7) [29] as follows:

$$\mathbf{F}_{\text{int},e} = ALS\frac{\partial \varepsilon}{\partial \mathbf{u}_e}. \tag{10}$$

2.2. Small Deformations—Linear Truss Formulation. In many engineering applications, only small deformations and strains occur. For these application cases, a simplified element formulation can be applied, facilitating both the derivation as well as the implementation. The small deformations and strains allow the use of the linear elastic Hooke's law to express the axial stress σ by the Young's Modulus E and the linear axial strain ϵ

$$\begin{aligned} \sigma &= E\epsilon, \\ \epsilon &= \frac{\partial u}{\partial X}. \end{aligned} \tag{11}$$

Here, u is the axial displacement field, and X is the coordinate running along the local element axis in its reference configuration. The strains and deformations are thus restricted to be small.

2.2.1. Stiffness Matrix in 1D. We start the derivation in 1D which is here expressed for a one-dimensional truss element as shown in Figure 3. The two nodal dofs u_1, u_2 are sufficient to describe the local element displacement field.

The virtual internal work is again expressed by integrating over the reference volume V as follows:

$$\delta W_{\text{int}} = \int_V \sigma \delta \epsilon \, \mathrm{d}V. \tag{12}$$

This is used in conjunction with linear shape functions to derive the local one-dimensional element stiffness matrix$\mathbf{K}_e^l$,

$$\mathbf{K}_e^l = \frac{EA}{L}\begin{bmatrix} 1 & -1 \\ -1 & 1 \end{bmatrix}. \tag{13}$$

2.2.2. Rotation to 3D. To analyze a global three-dimensional problem, a third dof is introduced. As depicted in Figure 2, three dofs at each node describe the total elemental deformation capacities and are given in equation (1). The introduction of the three-dimensional dofs allows the expression of the one-dimensional local element stiffness matrix from equation (13) to the three-dimensional space

$$\mathbf{K}_e^l = \frac{EA}{L}\begin{bmatrix} 1 & 0 & 0 & -1 & 0 & 0 \\ 0 & 0 & 0 & 0 & 0 & 0 \\ 0 & 0 & 0 & 0 & 0 & 0 \\ -1 & 0 & 0 & 1 & 0 & 0 \\ 0 & 0 & 0 & 0 & 0 & 0 \\ 0 & 0 & 0 & 0 & 0 & 0 \end{bmatrix}. \tag{14}$$

as well as the transformation/rotation matrix $\mathbf{T}$ as follows:

$$\mathbf{T} = \begin{bmatrix} \mathbf{n}[0] & 0 & 0 & 0 & 0 & 0 \\ \mathbf{n}[1] & 0 & 0 & 0 & 0 & 0 \\ \mathbf{n}[2] & 0 & 0 & 0 & 0 & 0 \\ 0 & 0 & 0 & \mathbf{n}[0] & 0 & 0 \\ 0 & 0 & 0 & \mathbf{n}[1] & 0 & 0 \\ 0 & 0 & 0 & \mathbf{n}[2] & 0 & 0 \end{bmatrix}, \tag{15}$$

$$\mathbf{n}^T = \frac{\begin{bmatrix} dX & dY & dZ \end{bmatrix}}{L}.$$

The direction vector $\mathbf{n}$ is used to express the orientation of the truss in the three-dimensional space, see Figure 2. Combining the previously derived element matrices, $\mathbf{K}_e^l$ can be expressed with respect to the global, three-dimensional dofs to obtain the global element stiffness matrix 23.

$$\mathbf{K}_e^g = \mathbf{T}\mathbf{K}_e^l\mathbf{T}^T \tag{16}$$

Finally, the internal forces for the linear truss formulation are formulated as follows:

$$\mathbf{F}_{int,e} = \mathbf{K}_e^g\mathbf{u}_e. \tag{17}$$

3. Global Problem Formulation

3.1. Standard Static Force Equilibrium. First, the standard static force equilibrium in the reference configuration is expressed to proceed with the solution process of finding

Figure 3: Linear truss element with nodal degrees of freedom, 1D.

the unknown reference configuration. Then, following the FEM workflow, the global element stiffness matrices of all structural elements are assembled by their dof numbering. The dof-based assembly [31] is from here on described by the $\sum$ symbol, using a node n or an element e loop.

$$\begin{aligned} &\mathbf{K} = \sum_e \mathbf{K}_e^g, \quad \mathbf{F}_{ext} = \sum_n \mathbf{F}_{ext,n}, \quad \mathbf{F}_{\text{int}} = \sum_e \mathbf{F}_{\text{int},e}, \\ &\mathbf{u} = \sum_e \mathbf{u}_e, \quad \mathbf{x} = \sum_e \mathbf{x}_e, \quad \mathbf{X} = \sum_e \mathbf{X}_e. \end{aligned} \tag{18}$$

All stiffness matrices are assembled in the global system stiffness matrix $\mathbf{K}$, the internal element forces are assembled in the global internal force vector $\mathbf{F}_{int}$, and the external nodal forces are assembled in the global load vector $\mathbf{F}_{ext}$. While $\mathbf{F}_{ext}$ is, in general, assumed to be constant, later in Section 3.2.3, the influence of additional self-weight is discussed. Other entities, such as the nodal discrete displacements and coordinates, are as well assembled.

Finally, we can express the global force equilibrium of the whole system in equation (19). With the reference configuration$\mathbf{X}$describing the system unknowns the expression turns out to be nonlinear, allowing us to express a force residual$\mathbf{r}$equation.

$$\mathbf{F}_{\text{int}}(\mathbf{X}, \mathbf{x}) - \mathbf{F}_{\text{ext}} = \mathbf{r}(\mathbf{X}, \mathbf{x}). \tag{19}$$

Note: For in a standard static analysis$\mathbf{x}$and thus the nodal displacements$\mathbf{u}$, would be the unknown vector. The standard problem assumes a given (known) reference configuration and solves the force equilibrium in (19) for the unknown displacements.

3.2. Inverse Problem. For the problem at hand, however, the unknown is the reference configuration $\mathbf{X}$, making it necessary to solve a system of nonlinear equations. Figure 4 demonstrates the inverse problem, depicting the known deformed configuration $\mathbf{x}$ and the unknown reference configuration $\mathbf{X}$.

We propose to use a Newton–Raphson solution scheme, expressing (19) in the form of a truncated Taylor's series, with k being the current iteration number

$$\mathbf{r}^{k+1} = \mathbf{r}^k + \overbrace{\frac{\partial \mathbf{r}^k}{\partial \mathbf{X}}}^{\mathbf{C}^k} \Delta \mathbf{X}^k = \mathbf{0}. \tag{20}$$

The necessary derivative of the residual vector is introduced to be the $\mathbf{C}$ system matrix

$$\Delta \mathbf{X}^k = \mathbf{X}^{k+1} - \mathbf{X}^{\mathrm{k}} = -\mathbf{C}^{-1^{\mathrm{k}}} \mathbf{r}^{\mathrm{k}}. \tag{21}$$

which is as well assembled by individual element e contributions

$$\mathbf{C} = \sum_e \mathbf{C}_e. \tag{22}$$

The following two Sections 3.2.1 and 3.2.2 discuss the necessary steps to formulate $\mathbf{C}_e$ assembled in equation (22).

3.2.1. Large Deformations—Nonlinear Truss Formulation. With respect to the global force equilibrium in (19), the element residual contribution is formulated as

$$\mathbf{r}_e = \mathbf{F}_{\text{int},e} = ALS \frac{\partial \varepsilon}{\partial \mathbf{u}_e}, \tag{23}$$

which is derived in equation (10).

The element solution matrix $\mathbf{C}_e$ is consequently derived by differentiating the element residual $\mathbf{r}_e$ with respect to the unknown reference configuration $\mathbf{X}$.

$$\begin{aligned} \mathbf{C}_e &= \frac{\partial \mathbf{r}_e}{\partial \mathbf{X}_e} = \frac{\partial \mathbf{F}_{\text{int},e}}{\partial \mathbf{X}_e}, \\ &= \underbrace{A S \frac{\partial \varepsilon}{\partial \mathbf{u}_e} \frac{\partial L}{\partial \mathbf{X}_e}}_{I} \\ &\quad + \underbrace{A L \frac{\partial \varepsilon}{\partial \mathbf{u}_e} \frac{\partial S}{\partial \mathbf{X}_e}}_{II} \\ &\quad + \underbrace{A L S \frac{\partial^2 \varepsilon}{\partial \mathbf{u}_e \partial \mathbf{X}_e}}_{III}. \end{aligned} \tag{24}$$

(24) can be split into three parts $I - III$ and will be accordingly formulated for clarity in the following.

Part I

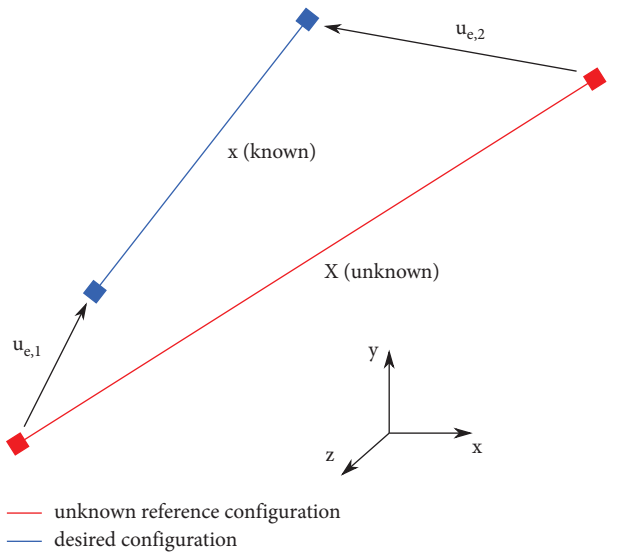

Figure 4: Unknown reference configuration deforms to the desired configuration.

$$\frac{\partial \varepsilon}{\partial \mathbf{u}_e} = \frac{\partial \varepsilon}{\partial l}\frac{\partial l}{\partial \mathbf{u}_e}$$

$$\frac{\partial \varepsilon}{\partial l} = \frac{l}{L^2},$$

$$\frac{\partial l}{\partial \mathbf{u}_e} = \frac{1}{l} d\mathbf{x}_e, \tag{25}$$

$$\frac{\partial L}{\partial \mathbf{X}_e} = \frac{1}{L} d\mathbf{X}_e.$$

$$\begin{aligned} d\mathbf{x}_e &= [\,-dx \;\; -dy \;\; -dz \;\; dx \;\; dy \;\; dz\,], \\ d\mathbf{X}_e &= [\,-dX \;\; -dY \;\; -dZ \;\; dX \;\; dY \;\; dzZ\,], \end{aligned} \tag{26}$$

Part II

$$\frac{\partial S}{\partial X_e} = \overbrace{\frac{\partial S}{\partial \varepsilon}}^{C}\frac{\partial \varepsilon}{\partial X_e} = C\frac{\partial \varepsilon}{\partial L}\frac{\partial L}{\partial X_e} + \underbrace{C\frac{\partial \varepsilon}{\partial l}\frac{\partial l}{\partial X_e}}_{=0,\ \text{const.}}, \tag{27}$$

$$\frac{\partial \varepsilon}{\partial L} = -\frac{l^2}{L^3}.$$

Part III

$$\frac{\partial^2 \varepsilon}{\partial u_e \partial X_e} = \frac{\partial}{\partial X_e}\left(\frac{\partial \varepsilon}{\partial l}\frac{\partial l}{\partial u_e}\right),$$

$$= \frac{\partial l}{\partial u_e}\frac{\partial^2 \varepsilon}{\partial l \partial Xe} + \underbrace{\frac{\partial \varepsilon}{\partial l}\frac{\partial^2 l}{\partial u_e \partial X_e}}_{=0,\ \text{const.}} \tag{28}$$

$$\frac{\partial^2 \varepsilon}{\partial l \partial Xe} = \frac{\partial}{\partial X_e}\frac{\partial \varepsilon}{\partial l} = \frac{\partial}{\partial X_e}\frac{l}{L^2},$$

$$= \left(\frac{\partial}{\partial L}\frac{l}{L^2}\right)\frac{\partial L}{\partial X_e} + \underbrace{\left(\frac{\partial}{\partial l}\frac{l}{L^2}\right)\frac{\partial l}{\partial X_e}}_{=0,\ \text{const.}}, \tag{29}$$

$$= -\frac{2l}{L^3}\frac{\partial L}{\partial X_e}$$

The preceding derivations allow the expression of the element solution matrix $\mathbf{C}_e$ for arbitrary hyperelastic material laws. Depending on the chosen material law, the 2 nd Piola-Kirchhoff stress S and the appropriate material tangent modulus $\mathbb{C}$ need to be calculated. For a selected choice of suitable material models, Section 2.1 provides the necessary terms.

3.2.2. Small Deformations—Linear Truss Formulation. Following the internal force expression for small deformations in (17), the elemental residual is expressed as

$$\mathbf{r}_e = \mathbf{F}_{\text{int},e} = \mathbf{K}_e^g \mathbf{u}_e. \tag{30}$$

Combining equations (1-3), the nodal dofs are expressed via the difference between the reference and the actual configuration in equation (31). This step is especially important as the reference configuration is unknown in this work, see Figure 4.

$$\mathbf{u}_e = [\,x_1 - X_1 \;\; y_1 - Y_1 \;\; z_1 - Z_1 \;\; x_2 - X_2 \;\; y_2 - Y_2 \;\; z_2 - Z_2\,]. \tag{31}$$

The Solution Matrix $\mathbf{C}_e$: From (19), it can be seen that the derivative of the residual with respect to the unknown configuration results in a nonlinear problem. Following (22), the elemental solution matrix $\mathbf{C}_e$ is in the following derived on element level. Applying the chain rule to the internal element residual in equation (30).

$$\begin{aligned} \mathbf{C}_e &= \frac{\partial \mathbf{r}_e}{\partial \mathbf{X}_e} \\ &= \frac{\partial \mathbf{K}_e^g}{\partial \mathbf{X}_e}\mathbf{u}_e + \mathbf{K}_e^g \underbrace{\frac{\partial \mathbf{u}_e}{\partial \mathbf{X}_e}}_{-\mathbf{I}} \\ &= \frac{\partial \mathbf{K}_e^g}{\partial \mathbf{X}_e}\mathbf{u}_e - \mathbf{K}_e^g \\ &= \widehat{\mathbf{K}}_e^g \widehat{\mathbf{u}}_e - \mathbf{K}_e^g. \end{aligned} \tag{32}$$

The new tensors $\widehat{\mathbf{K}}_e^g, \widehat{\mathbf{u}}_e$ are introduced for simplification and are described in the following. This notation allows a straightforward description of the remaining operations. $\widehat{\mathbf{u}}_e$ will result in a 36×6 matrix, with the elemental nodal displacement vector $\mathbf{u}_e$ moving from the very left top to the right bottom

$$\widehat{\mathbf{u}}_e = \begin{bmatrix} \mathbf{u}_e & \mathbf{0} & \mathbf{0} & \mathbf{0} & \mathbf{0} & \mathbf{0} \\ \mathbf{0} & \mathbf{u}_e & \mathbf{0} & \mathbf{0} & \mathbf{0} & \mathbf{0} \\ \mathbf{0} & \mathbf{0} & \mathbf{u}_e & \mathbf{0} & \mathbf{0} & \mathbf{0} \\ \mathbf{0} & \mathbf{0} & \mathbf{0} & \mathbf{u}_e & \mathbf{0} & \mathbf{0} \\ \mathbf{0} & \mathbf{0} & \mathbf{0} & \mathbf{0} & \mathbf{u}_e & \mathbf{0} \\ \mathbf{0} & \mathbf{0} & \mathbf{0} & \mathbf{0} & \mathbf{0} & \mathbf{u}_e \end{bmatrix}. \tag{33}$$

At the same time, $\widehat{\mathbf{K}}_e^g$ can be expressed with the help of the single respective derivative of the global element stiffness

matrix, with respect to each unknown reference position in space, resulting in a 6×36 matrix

$$\widehat{\mathbf{K}}_e^g = \left[\frac{\partial \mathbf{K}_e^g}{\partial X_1} \; \frac{\partial \mathbf{K}_e^g}{\partial Y_1} \; \frac{\partial \mathbf{K}_e^g}{\partial Z_1} \; \frac{\partial \mathbf{K}_e^g}{\partial X_2} \; \frac{\partial \mathbf{K}_e^g}{\partial Y_2} \; \frac{\partial \mathbf{K}_e^g}{\partial Z_2} \right]. \tag{34}$$

The individual derivative expressions in (34) are calculated by the chain rule applied to (16) including the derivatives of the transformation matrix and the local element stiffness matrix.

Derivatives of $\mathbf{K}_e^g$: The respective derivatives in (34) are discussed in the following, rearranging the global element stiffness matrix from (16) by merging the length terms

$$\mathbf{K}_e^g = \mathbf{T}\mathbf{K}_e^l\mathbf{T}^T = \frac{EA}{L^3}\overline{\mathbf{T}}\overline{\mathbf{K}}_e^l\overline{\mathbf{T}}^T. \tag{35}$$

The $\overline{\bullet}$ matrices are obtained by multiplying the original matrices by the length L, so that the length is separated as shown in (35), rendering a constant matrix $\overline{\mathbf{K}}_e^l$.

Now, the derivative of $\mathbf{K}_e^g$ with respect to an arbitrary reference coordinate X_i can finally be expressed as follows:

$$\frac{\partial \mathbf{K}_e^g}{\partial X_i} = -\frac{3EA}{L^4}\frac{\partial L}{\partial X_i}\overline{\mathbf{T}}\overline{\mathbf{K}}_e^l\overline{\mathbf{T}}^T + \frac{EA}{L^3}\left(\frac{\partial \overline{\mathbf{T}}}{\partial X_i}\overline{\mathbf{K}}_e^l\overline{\mathbf{T}}^T + \overline{\mathbf{T}}\overline{\mathbf{K}}_e^l\frac{\partial \overline{\mathbf{T}}^T}{\partial X_i}\right). \tag{36}$$

First, the derivative of the length with respect to the reference coordinates can be written in the following form and will later be used again, when including self-weight

$$\begin{aligned}\frac{\partial L}{\partial \mathbf{X}_e} &= \left[\frac{\partial L}{\partial X_1} \; \frac{\partial L}{\partial Y_1} \; \frac{\partial L}{\partial Z_1} \; \frac{\partial L}{\partial X_2} \; \frac{\partial L}{\partial Y_2} \; \frac{\partial L}{\partial Z_2} \right], \\ &= \frac{\left[-dX \;\; -dY \;\; -dZ \;\; +dX \;\; +dY \;\; +dZ \right]}{L}.\end{aligned} \tag{37}$$

Additionally, the derivative of the transformation matrix $\overline{\mathbf{T}}$, which has the length excluded, results in the following simple matrices:

$$\begin{aligned}\frac{\partial \overline{\mathbf{T}}}{\partial X_1} &= -\frac{\partial \overline{\mathbf{T}}}{\partial X_2} \\ &= \begin{bmatrix} -1 & 0 & 0 & 0 & 0 & 0 \\ 0 & 0 & 0 & 0 & 0 & 0 \\ 0 & 0 & 0 & 0 & 0 & 0 \\ 0 & 0 & 0 & -1 & 0 & 0 \\ 0 & 0 & 0 & 0 & 0 & 0 \\ 0 & 0 & 0 & 0 & 0 & 0 \end{bmatrix}, \\ \frac{\partial \overline{\mathbf{T}}}{\partial Y_1} &= -\frac{\partial \overline{\mathbf{T}}}{\partial Y_2} \\ &= \begin{bmatrix} 0 & 0 & 0 & 0 & 0 & 0 \\ -1 & 0 & 0 & 0 & 0 & 0 \\ 0 & 0 & 0 & 0 & 0 & 0 \\ 0 & 0 & 0 & 0 & 0 & 0 \\ 0 & 0 & 0 & -1 & 0 & 0 \\ 0 & 0 & 0 & 0 & 0 & 0 \end{bmatrix}, \\ \frac{\partial \overline{\mathbf{T}}}{\partial Z_1} &= -\frac{\partial \overline{\mathbf{T}}}{\partial Z_2} \\ &= \begin{bmatrix} 0 & 0 & 0 & 0 & 0 & 0 \\ 0 & 0 & 0 & 0 & 0 & 0 \\ -1 & 0 & 0 & 0 & 0 & 0 \\ 0 & 0 & 0 & 0 & 0 & 0 \\ 0 & 0 & 0 & 0 & 0 & 0 \\ 0 & 0 & 0 & -1 & 0 & 0 \end{bmatrix}. \end{aligned} \tag{38}$$

3.2.3. Including Self-Weight. Additional terms need to be considered when including self-weight. As the self-weight depends on the reference element length, the unknown reference configuration influences the load case and adds new nonlinear terms to $\mathbf{r}_e$.

With the help of the mass density ρ and a global gravity-direction vector $\mathbf{g}$, the additional nodal forces per element are expressed as follows:

$$\begin{aligned}\mathbf{F}_{\text{gravity},e} &= 0.5\overbrace{\rho A L(\mathbf{X})}^{\text{mass}(\mathbf{X})}\mathbf{g}\, g_{\text{earth}}, \\ \mathbf{g}^T &= \left[g_x \;\; g_y \;\; g_z \;\; g_x \;\; g_y \;\; g_z \right].\end{aligned} \tag{39}$$

With g_x, g_y, g_z being the spatial components of the normalized gravity direction vector and the gravitational acceleration $g_{\text{earth}} \approx 9.81 m/s^2$. Additionally, to the previously derived element residual $\mathbf{r}_e$, the self-weight forces need to be included

$$\mathbf{r}_e = \mathbf{F}_{\text{int},e} - \mathbf{F}_{\text{gravity},e}, \tag{40}$$

adding a new term to the element solution matrix $\mathbf{C}_e$. The following equation describes the complete matrix, including all necessary derivatives

$$\mathbf{C}_e = \frac{\partial \mathbf{F}_{\text{int},e}}{\partial \mathbf{X}_e} - \frac{\partial \mathbf{F}_{\text{gravity},e}}{\partial \mathbf{X}_e}. \tag{41}$$

With the help of the length derivatives in equation (35), the new term is calculated as follows:

$$\frac{\partial \mathbf{F}_{\text{gravity},e}}{\partial \mathbf{X}_e} = 0.5\,\rho A\,\mathbf{g}\,g_{\text{earth}}\,\frac{\partial L}{\partial \mathbf{X}_e}. \tag{42}$$

The additional terms to $\mathbf{C}_e$ in (41) hold for both the linear and the nonlinear truss element.

3.2.4. Code Implementation. In order to generate lasting added value, all derivatives are made publicly available. They can be downloaded as Python code via a GitHub repository [28]. Jupyter Notebook files are included for a direct assessment of all derivatives, functions, and the proceeding examples.

4. Examples

Several examples are presented in the following chapter. We will employ the derived system matrices in two and three dimensions. While smaller examples serve as an introduction, more complex systems are analyzed to demonstrate the simulation capabilities. For selected examples, a discussion of the solution convergence is added. While we present the nodal solutions for small examples, the solutions for large examples are only visualized. Additionally, all chosen stiffness and force values are purely academic. Forces are given in Newton N, distances and lengths in meter m, areas in m^2, and densities in kg/m^3. In the respective two-dimensional examples, the third direction, here the global z-axis, is fixed on all system nodes to prevent any movement in said direction.

This section includes the following examples:

(i) Section 4.1 demonstrates a simple 2D 3-bar system. The nonlinear solution is compared to the linear formulation, and convergence rates are included.

(ii) Section 4.2 discusses a 2D framework bridge. The nonlinear solution is compared to the linear formulation.

(iii) Section 4.3 analyses a 3D 3-bar system. The nonlinear solution is compared to the linear formulation.

(iv) Section 4.4 demonstrates a 3D frame. The nonlinear solution is compared to the linear formulation.

(v) Section 4.5 discusses a 3D framework bridge.

(vi) Section 4.6 shows a 3D 3-bar system, including self-weight. The nonlinear solution is compared to the linear formulation, and convergence rates are included.

(vii) Section 4.7 discusses the influence of different material laws on a 3D system.

(viii) Section 4.8 demonstrates a large structural setup with an increased number of degrees of freedom.

To verify the found reference configurations, a standard FEM analysis is performed on the found reference configuration. The results coincide with the desired final configuration and are visualized in most of the example discussions in this work. These standard FEM analyses have been performed with the code available in the GitHub repository [28] and verified with the open-source multiphysics software KRATOS [32–34].

All examples are accessible via a GitHub repository [28]. The interested reader is invited to download the offered files, re-run the examples herein, and analyze new structures. A tutorial is included, describing the proper usage.

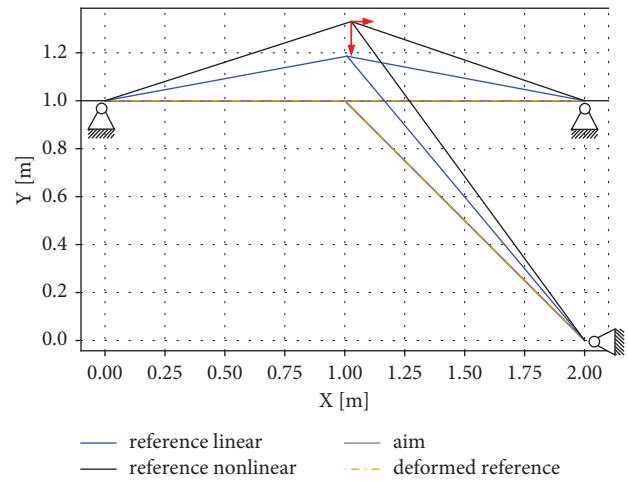

Figure 5: Unknown and known configuration of a 3-bar structure. The red arrows demonstrate the force vector.

4.1. 2D 3-Bar System. The first two-dimensional system describes a 3-bar structure as visualized in Figure 5. The Young's modulus E is chosen to be $1e6N/m^2$, and the cross section is $A = 1e{-}2\text{m}^2$, while the force vector on the free middle note is $[4e2, -8e2]N$. The St. Venant-Kirchhoff material law is used for the nonlinear truss formulation, and the standard, small deformation Hooke's law is for the linear truss formulation.

In Figure 5, the gray line presents the known deformed configuration, while the solid black and blue lines are the results of the inverse analyses herein. The different resulting reference configurations for the linear and the nonlinear truss formulation can be observed. While the linear truss formulation calculates the force equilibrium in the reference configuration and is restricted to small deformations, the nonlinear truss formulation formulates its force equilibrium in the deformed configuration and can represent large deformations. Additionally, the dotted yellow line describes the result of a standard FEM analysis on the found, previously unknown reference configurations. It can be observed that the solution of the standard FEM analysis coincides with the given desired aim configuration of the inverse analysis.

The found reference configuration of the middle free node is given in the following Table 1.

Additionally, Figure 6 presents the convergence of the problem residual with respect to the Newton-Raphson iterations k. The L − 2 norm $\|\bullet\|_2$ is chosen to depict a convergence rate that is at least quadratic.

Table 1: Solution of the initially unknown and known configuration of the 3-bar structure in Figure 5.

	X	Z	x	z
Linear	1.0093919774375	1.1858502537476	1.0	−1.0
Nonlinear	1.0273412684167	1.3304932012403	1.0	−1.0

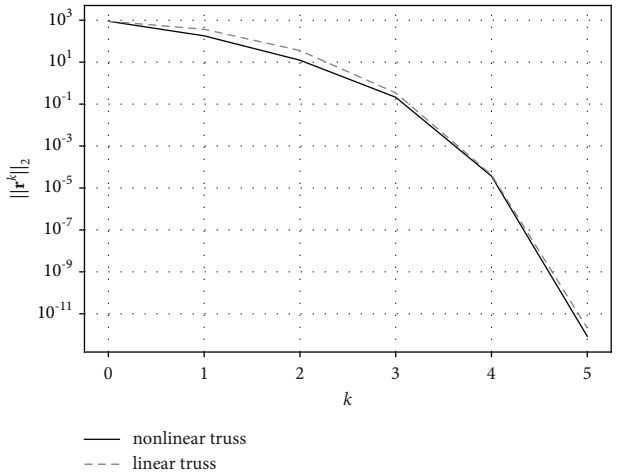

Figure 6: Convergence of the 3-bar system.

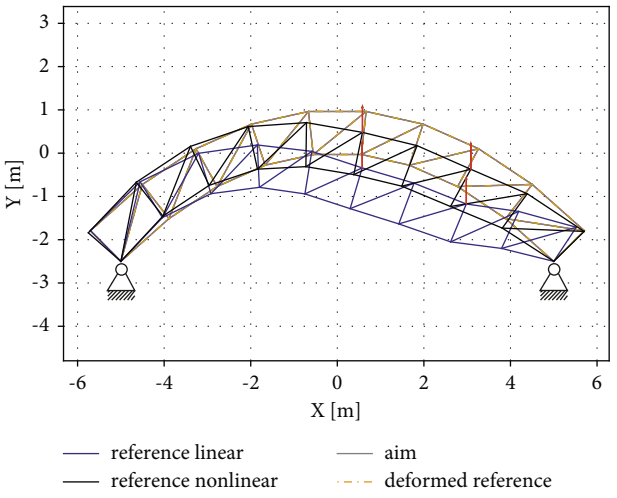

Figure 7: Unknown and known configuration of a two-dimensional bridge structure. The red arrows demonstrate the force vector.

4.2. 2D Framework Bridge. A truss framework bridge is modeled using multiple structural elements in two dimensions. The structure in Figure 7 has a Young's modulus $E = 3e5N/m^2$, a cross section$A = 1e{-}2\text{m}^2$, and two vertical forces in y-direction of magnitude $1e2N$. The forces are intentionally chosen to be arbitrary and nonsymmetric to test the simulation capabilities. The St. Venant-Kirchhoff material law is used for the nonlinear truss formulation, and the standard, small deformation Hooke's law is for the linear truss formulation. Figure 7 nicely shows the solution for the unknown

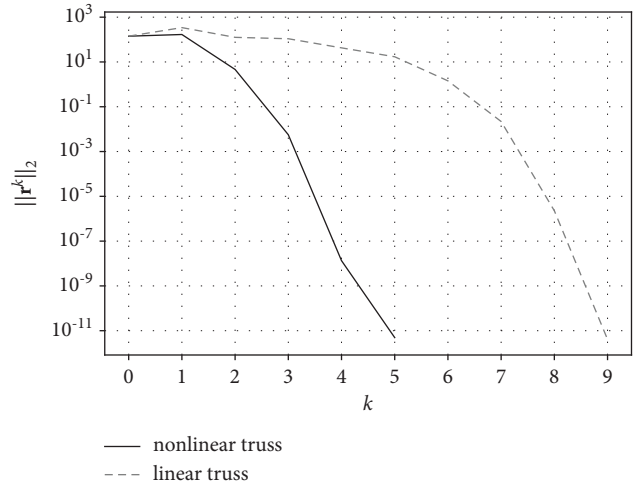

Figure 8: Convergence of the 2D framework bridge system.

reference configuration and the result of a proceeding standard FEM analysis. The found reference shapes deform nicely into the desired aim configuration. The difference between the linear and nonlinear truss formulation again can be observed. Figure 8 presents the course of the residual over iterations steps k. The gradient for $\|\mathbf{r}^k\|_2 < 1e-1$ demonstrates the correct implementation.

4.3. 3D 3-Bar System. To begin with 3D systems, a 3-bar structure is investigated. The structure has a Young's modulus $E = 1e6N/m^2$, a cross section$A = 1e{-}2\text{m}^2$, and a force vector of $[1e3, 0, 2e3]N$ is applied to the free node. The St. Venant-Kirchhoff material law is used for the nonlinear truss formulation, and the standard, small deformation Hooke's law is for the linear truss formulation. Solutions for the unknown reference configuration are visualized in Figure 9 and given in Tables 2 and 3.

The found reference configuration of the middle free node is given in the following.

Again, Figure 10 presents the convergence for both the linear and the nonlinear truss elements.

4.4. 3D Frame. Figure 11 depicts the next three-dimensional setup. The frame is supposed to deflect to a regular rectangular shape, as demonstrated by the gray dotted lines. The system uses a Young's modulus $E = 1e6N/m^2$ and a cross section$A = 1e{-}2\text{m}^2$, and the nodal force vector is $[300, 300, 300]N$. The St. Venant-Kirchhoff material law is used for the nonlinear truss formulation, and the standard, small deformation Hooke's law is for the linear truss formulation.

The respective convergence rates are given in Figure 12.

4.5. 3D Framework Bridge. Subsequently, we present the example of a 3D framework bridge structure, as shown in Figure 13. While a single force loads the structure nonsymmetric with $[0, -800, 0]N$, the system's Young's

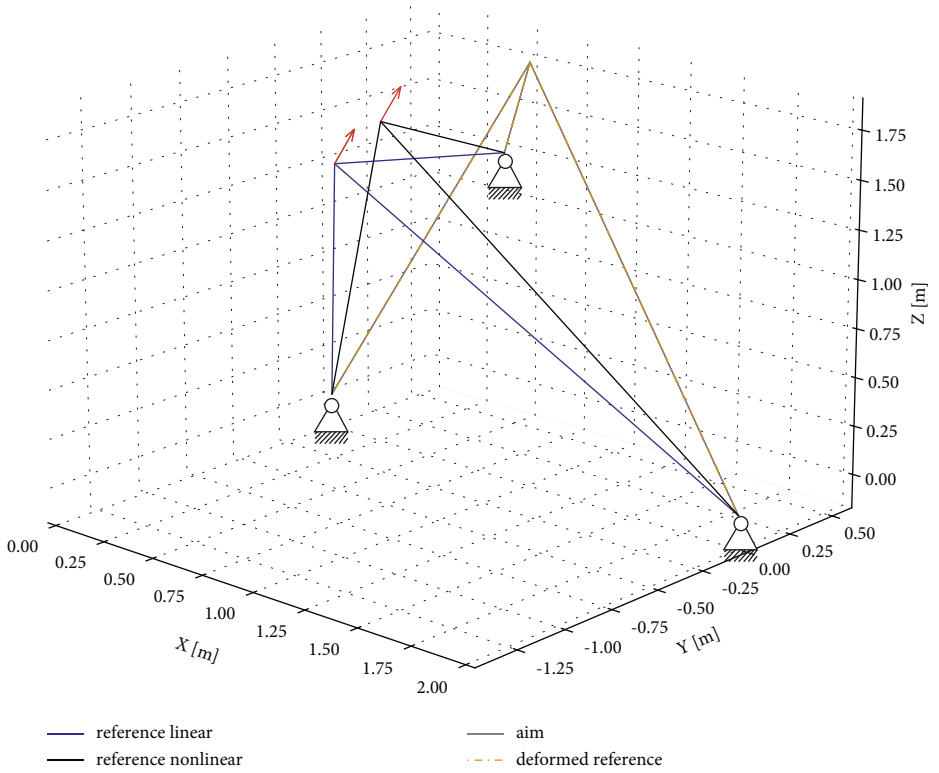

Figure 9: Unknown and known configuration of a 3-bar structure. The red arrow demonstrates the force vector $[1e3, 0, 2e3]N$.

Table 2: Solution of the initially unknown configuration and aim configuration of the 3-bar structure in Figure 9 with linear truss elements.

X	Y	Z
0.4775519165819412	−0.48025726960289933	1.4935108461479483
x	y	z
1.0	0.0	2.0

Table 3: Solution of the initially unknown configuration and aim configuration of the 3-bar structure in Figure 9 with nonlinear truss elements.

X	Y	Z
0.6553972454362691	−0.424638016434548	1.735432507307086
x	y	z
1.0	0.0	2.0

modulus is $E = 1e7N/m^2$, and the elements are assigned a cross section$A = 1e{-}2\text{m}^2$. The St. Venant-Kirchhoff material law is used for the nonlinear truss formulation, and the standard, small deformation Hooke's law is for the linear truss formulation. As the three dimensionality makes a proper visualization difficult, the found reference configuration is compared to the desired aim configuration in multiple spatial projections. Figure 13 depicts a three-dimensional side view.

Figures 14 and 15 show a projection in the $x - z$ plane for different levels of z. The vertical point load of −800 N in y-direction is visualized in Figure 15.

In the following Figures 16 and 17, the projection on the $x - z$ plane is shown for different y levels.

The convergence rate for the 3D bridge system is visualized in Figure 18. While the linear truss formulation needs several iterations to reach $\|\mathbf{r}^k\|_2 < 1e - 1$, it thereafter shows proper convergence.

4.6. Self-Weight. In the following, the inclusion of the self-weight is discussed with respect to the problem solving procedure. The same 3-bar system as in Section 4.3 is used with$E = 1e6N/m^2$, $A = 1e{-}2\text{m}^2$, $\mathbf{g} = [0, 1, 0]$, and $\rho = 1e3kg/m^3$. The St. Venant-Kirchhoff material law is used for the nonlinear truss formulation, and the standard, small deformation Hooke's law is for the linear truss formulation. The theoretical background and the respective symbols are

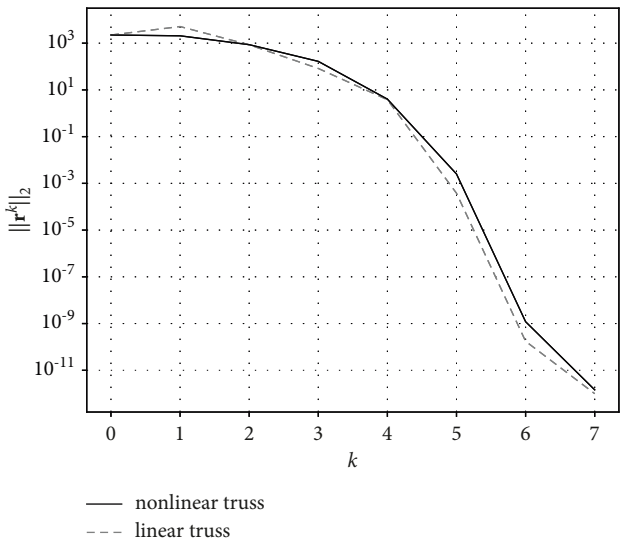

Figure 10: Convergence of the 3D 3-bar system.

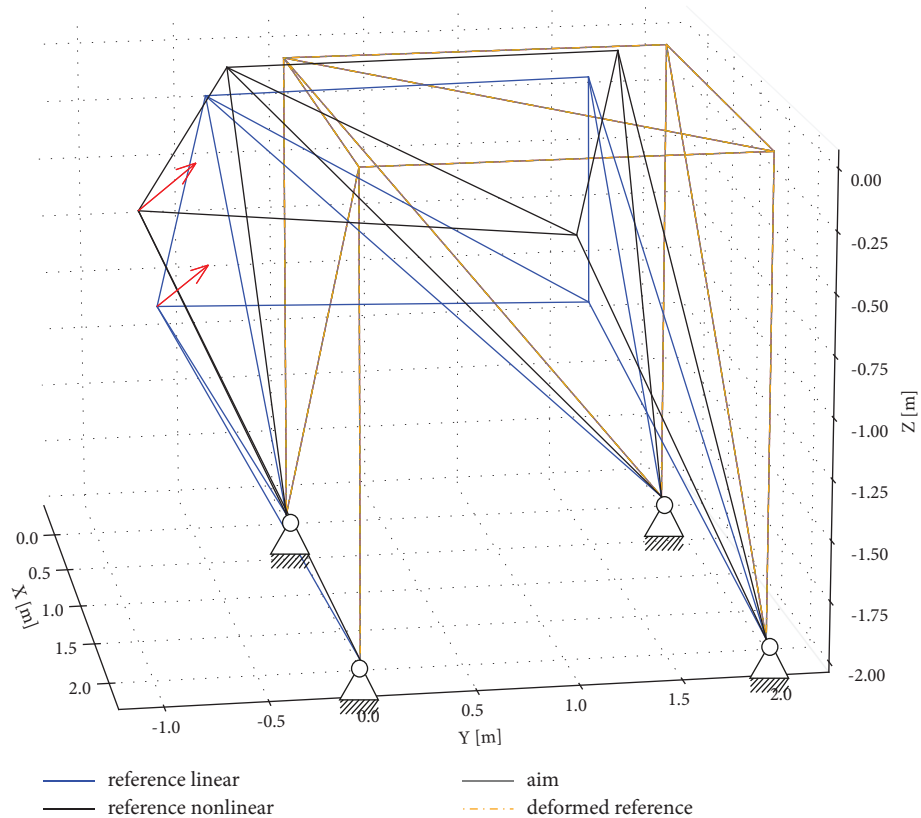

Figure 11: Unknown and known configuration of a three-dimensional frame structure. The red arrow demonstrates the force vector $[300, 300, 300]N$.

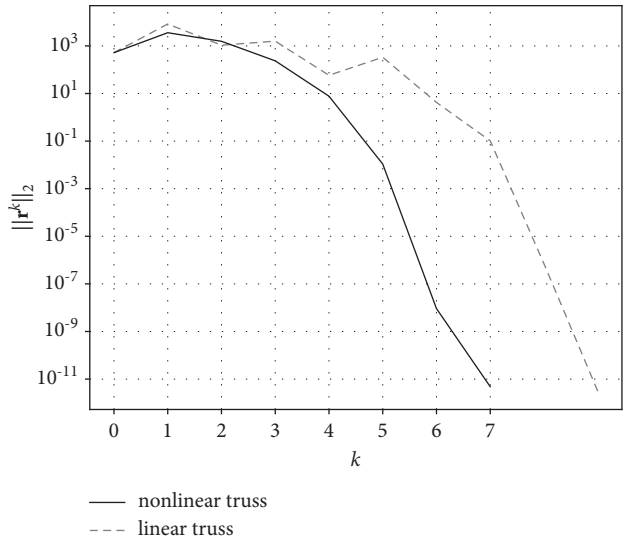

Figure 12: Convergence of the 3D frame system.

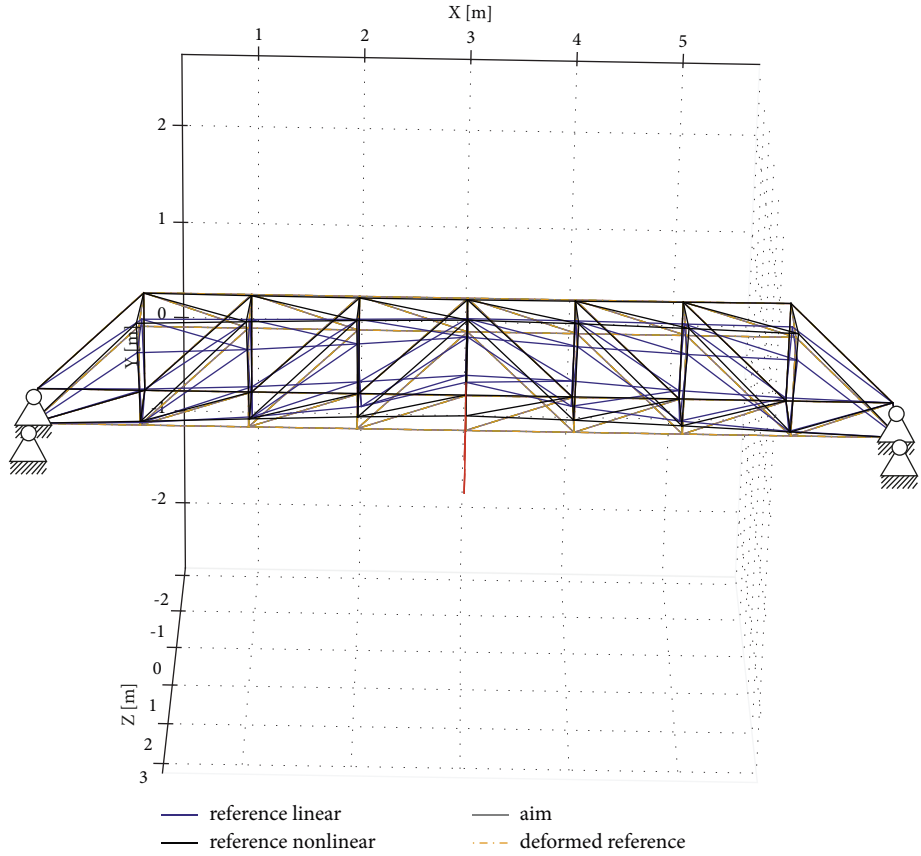

Figure 13: Unknown and known configuration of a 3D bridge structure. The red arrow demonstrates the force vector $[0, -800, 0]N$.

discussed in Section 3.2.3. Figure 19 visualizes the problem setup and the found, initially unknown reference configuration in the following.

After solving for the unknown reference configuration, the following discrete nodal position is found. Table 4 presents the result for the linear truss formulation, while Table 5 relates to the nonlinear formulation.

While the inclusion of the self-weight leads to additional forces, it influences the setup of the solution matrix $\mathbf{C}_e$, too. The necessary changes to $\mathbf{C}_e$ are discussed in Section 3.2.3, especially in equation (39). While, in some cases, it is also possible to find a solution for the self-weight problem employing the original matrix from equations (27) or (32), a lower convergence rate is

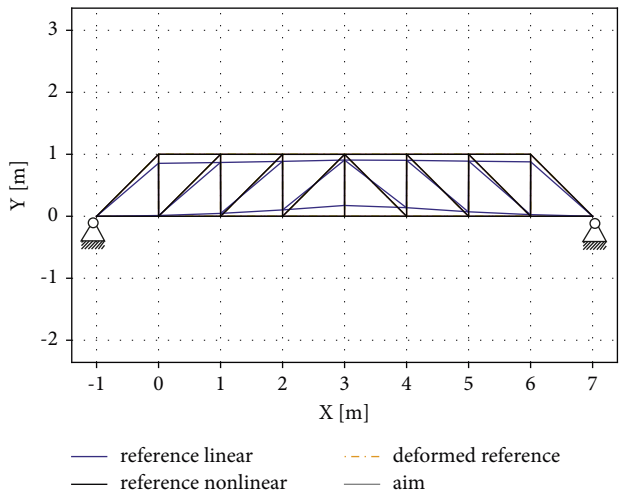

Figure 14: Bridge configurations in $x - y$ plane for $z = 0$.

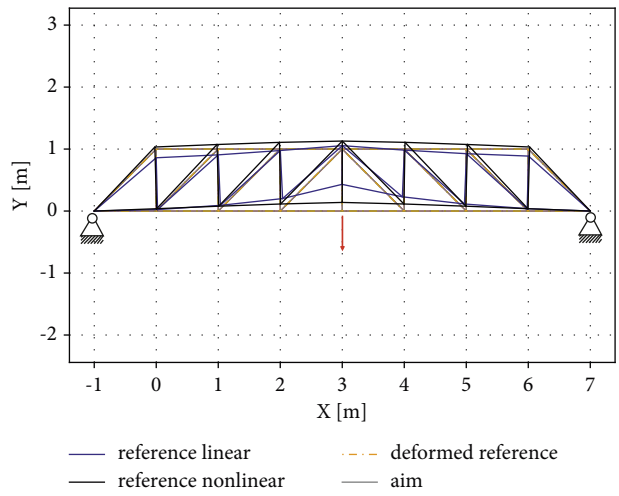

Figure 15: Bridge configurations in $x - y$ plane for $z = 1$. The red arrow describes the vertical point load.

expected. This behavior is visualized in Figure 20, where the same problem is solved twice. Ones, using the original matrix from equation (30) for linear trusses and equation (29) for nonlinear trusses (here named "incomplete," due to its lack of necessary terms) and again with the complete matrix from equation (41). The latter equation includes all derivatives of the new residual vector, containing the self-weight loads dependent on the unknown reference configuration. The large differences in convergence rates can be seen in Figure 20, proving the correct derivation and implementation of the necessary additional derivative terms.

4.7. Different Hyperelastic Material Laws. To discuss the influence of the three different hyperelastic material laws introduced in Section 2.1, a 2D truss system is investigated, as depicted in Figure 21. The Young's modulus is always $E = 1e6N/m^2$, and the cross section is$A = 1e{-}2\text{m}^2$. While the St. Venant-Kirchhoff law and the Neo-Hookean law do not need further material parameters, $\beta_1 = 10, \beta_2 = 0$ is assigned to the Ogden law. Only the nonlinear truss formulation can be applied in conjunction with the nonlinear hyperelastic material laws. Figure 21 shows the different reference configurations for each of the material law. All three cases yield the desired aim configuration when simulated with a standard FEM analysis.

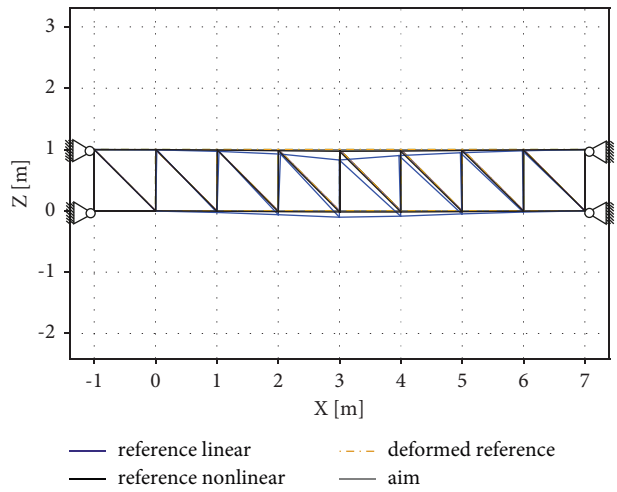

Figure 16: Bridge configurations in $x - z$ plane for $y = 0$.

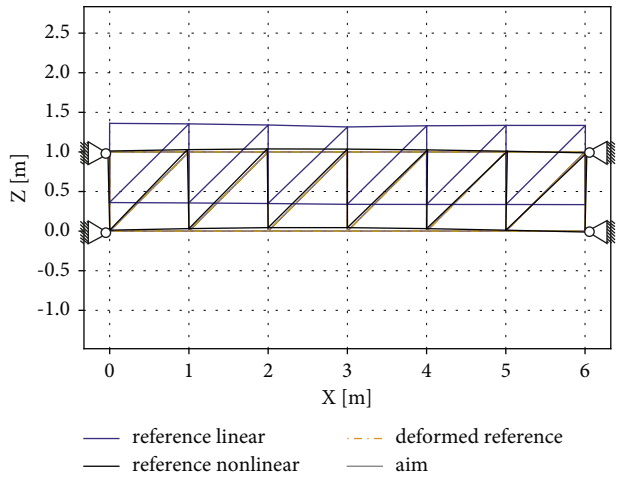

Figure 17: Bridge configurations in $x - z$ plane for $y = 1$.

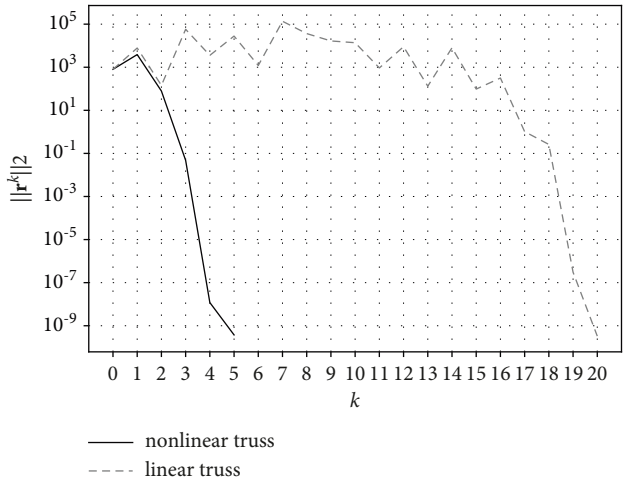

Figure 18: Convergence of the 3D bridge system.

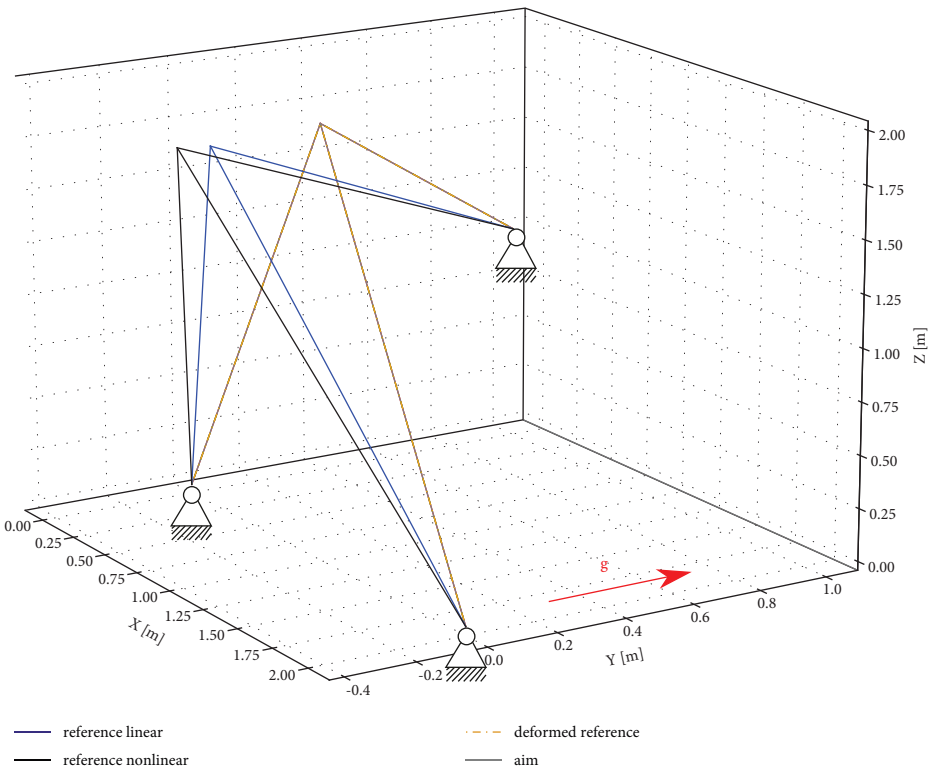

Figure 19: Unknown and known configuration of a three-dimensional truss structure, subjected to self-weight. The red arrow indicates the normalized gravity direction vector **g**, acting in the y-direction.

Table 4: Solution of the initially unknown configuration and aim configuration of the 3-bar structure in Figure 19 with linear truss elements.

X	Y	Z
0.874387790220	−0.2627503778460	1.9263479975443
x	y	z
1.0	0.0	2.0

Table 5: Solution of the initially unknown configuration and aim configuration of the 3-bar structure in Figure 19 with nonlinear truss elements.

X	Y	Z
0.8431479069299	−0.3437354017714	1.9298317925520
x	y	z
1.0	0.0	2.0

Figure 22 visualizes the convergence rate for each of the simulations. At least quadratic convergence is observed for all three cases.

The solution for the unknown reference configuration yields the following y-coordinate for the middle node, given in Table 6.

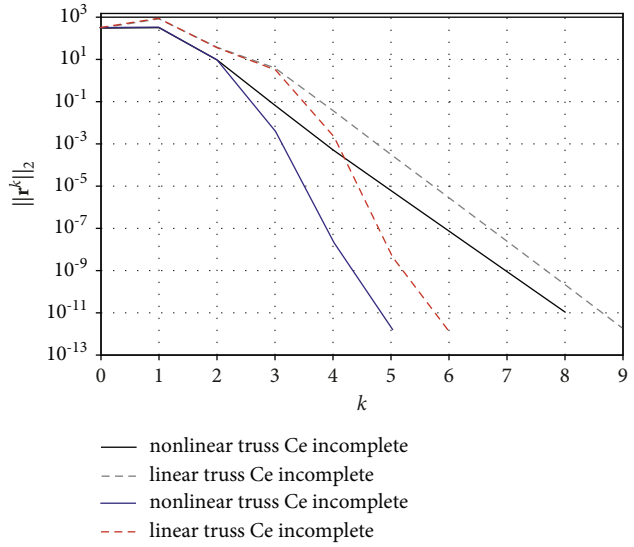

Figure 20: Convergence of the nonlinear self-weight problem, employing either the complete solution matrix $\mathbf{C}_e$ from equation 57 or the incomplete matrix from equation 32, respectively, 43. Both converge to the approximately same solution but show different convergence rates.

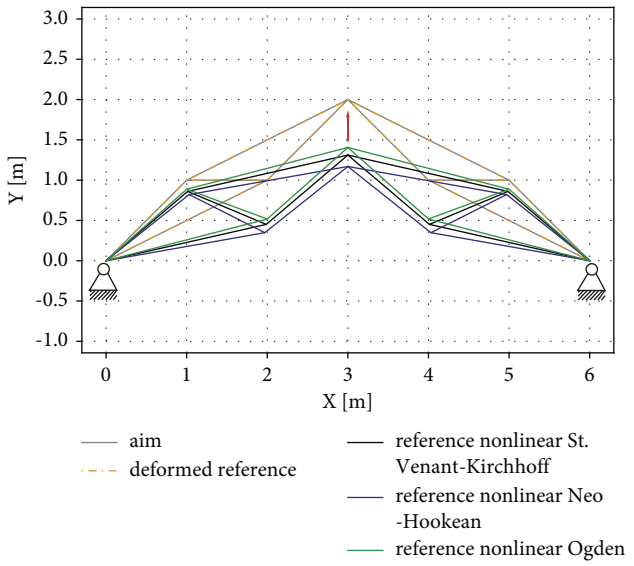

Figure 21: Unknown and known configuration of a 2D nonlinear truss structure. The three different hyperelastic material laws are compared: St. Venant-Kirchhoff, Neo-Hookean, Ogden.

Table 6: Unknown reference configuration and desired aim configuration for various hyperelastic material laws.

	St. Venant-Kirchhoff	Neo-Hookean	Ogden ($\beta_1 = 10, \beta_2 = 0$)
Y	2.0	2.0	2.0
Y	1.3113434128	1.1695200737	1.4055031762

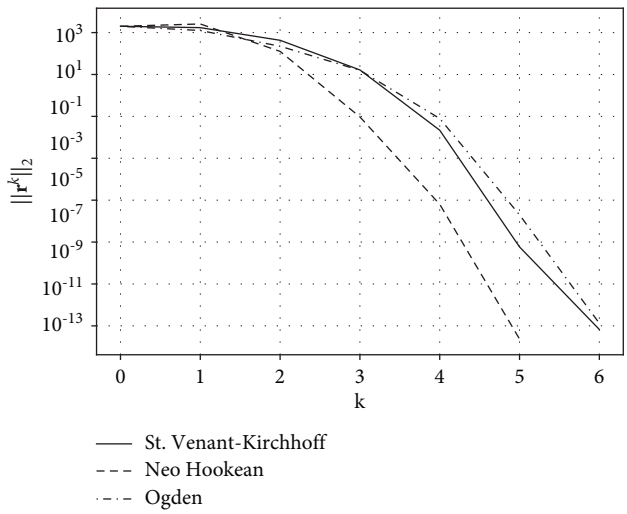

Figure 22: Convergence of the 2D nonlinear truss structure for different hyperelastic material laws.

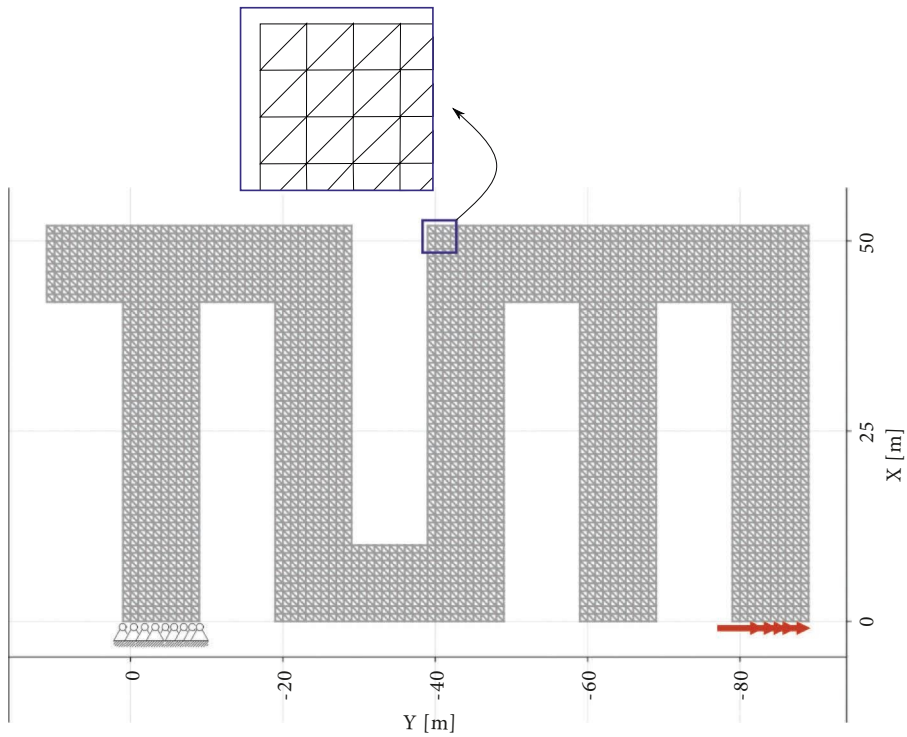

Figure 23: Known aim configuration. The whole model consists of single nonlinear truss elements, as depicted in the blue box. As all displacements out-of-plane are constrained, a total number of 3241 nodes yield $\approx 7e3$ dofs.

4.8. TUM Logo—Large Number of Degrees of Freedom. Finally, to conclude, we present an example with a larger number of dofs. The logo of the Technical University of Munich (TUM) is taken as an inspiration for the following example. As depicted in Figure 23, the whole structure is discretized with nonlinear truss elements, using the St. Venant-Kirchhoff material law. The Young's modulus is chosen to be $E = 2.069e11N/m^2$, and the cross section of each truss is$A = 1e{-}2\text{m}^2$. Supports are introduced on the left lower side as shown in Figure 23, and the right lower side is loaded with a y-load of $5e5N$ on 11 nodes. As all displacements in the global z-direction are fixed, the total number of 3241 nodes yields $\approx 7e3$ dofs.

Figure 24 finally visualizes the found reference configuration and the desired aim configuration, which coincides with the deformed reference structure, obtained by a standard FEM analysis on the found reference configuration.

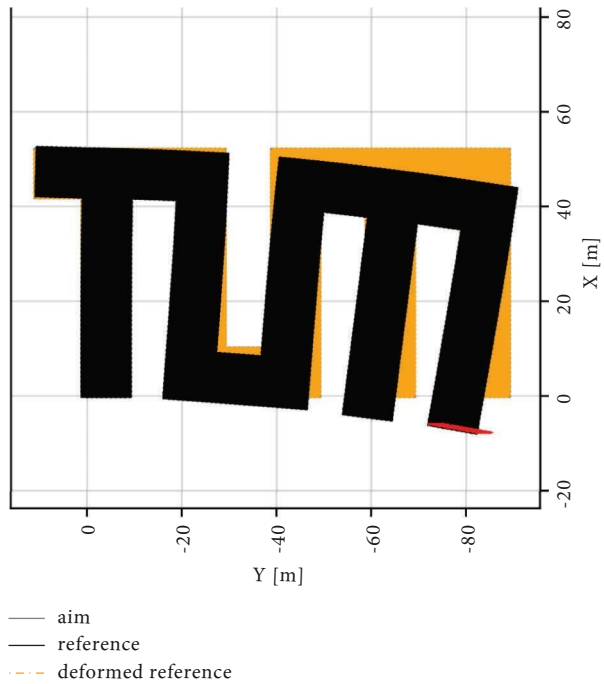

Figure 24: Unknown reference configuration and desired aim configuration for the nonlinear truss TUM logo. Boundary conditions are given in Figure 23.

5. Conclusion

In contrast to standard static analyses of structures, searching for a suitable reference geometry is not as straightforward. A reformulation of the structural force equilibrium equation is necessary. We are changing the unknowns from the structural displacements to the unknown reference configuration. This change of unknowns yields a different solution matrix, compared to the stiffness matrix of standard static analyses. Including load cases, which depend on the reference configuration (such as self-weight), adds additional nonlinear terms to the problem statement. This work presents the described problem reformulation in terms of unknowns for geometrically nonlinear truss elements combined with nonlinear hyperelastic material laws. Additionally, simplifications to linear truss formulations are given, offering a wide range of detailed derivations. To solve the newly obtained nonlinear system of equations, we propose the gradient-based Newton-Raphson solution scheme. Consequently, the preceding sections discuss and present arising system derivatives in great detail. Every part of each necessary solution matrix is derived and consequently given. Additionally, we published everything in a freely accessible GitHub repository [28]. While all system matrices are available, each presented example is added to the repository and thus freely available.

The derivation and implementation are checked by various two- and three-dimensional test cases, ranging from small systems to larger, more complex structures. The solution scheme herein, including all system matrices, can now be used to analyze workshop geometries for truss structures.

Abbreviations

FEM: Finite element method
Dof: Degree of freedom
VaReS: Variation of reference strategy
IBRA: Isogeometric B-Rep analysis
URS: Updated reference strategy
SGC: Statically geometrically coupled. Bold letters indicate vectors and tensors.

Data Availability

All matrices and presented examples are available in a GitHub repository: https://github.com/KlausBSautter/Find_Reference_Truss_3D.

Conflicts of Interest

The authors declare that they have no conflicts of interest.

Authors' Contributions

All authors prepared the manuscript. All authors read and approved the final manuscript.

References

[1] M. R. Barnes, "Form finding and analysis of tension structures by dynamic relaxation," *International Journal of Space Structures*, vol. 14, no. 2, pp. 89–104, 1999.

[2] M. Khatibinia, S. Hosseinaei, and S. R. Sarafrazi, "Efficiency of dynamic relaxation methods in form-finding of tensile membrane structures," *SN Applied Sciences*, vol. 1, no. 11, p. 1502, 2019.

[3] D. Wakefield, "Engineering analysis of tension structures: theory and practice," *Engineering Structures*, 1999.

[4] K. Linkwitz, *New Methods for the Determination of Cutting Pattern of Prestressed Cable Nets and Their Application to the Olympic Roofs München*, IASS Tokyo, Tokyo, Japan, 1971.

[5] K. Linkwitz and H.-J. Schek, *Über eine Methode zur Berechnung vorgespannter Seilnetze und ihre praktische Anwendung auf die Olympiadächer München*, IABSE, Zurich, Switzerland, 1972.

[6] H. J. Schek, "The force density method for form finding and computation of general networks," *Computer Methods in Applied Mechanics and Engineering*, vol. 3, no. 1, pp. 115–134, 1974.

[7] F. Leonhardt and J. Schlaich, *Weitgespannte Flächentragwerke [Long-Span Surface Structures]. [German], Sonderforschungsbericht [Special Research Report] 64*, Universität Stuttgart, Stuttgart, Germany, 1973.

[8] R. Kemmler, *Formfindung: Die Interaktion von Kraft und Geometrie [The Interaction of Force and Geometry] [German]*, Stahlbau, Kirchzarten, Germany, 2012.

[9] K.-U. Bletzinger and E. Ramm, "A general finite element approach to the form finding of tensile structures by the updated reference strategy," *International Journal of Space Structures*, vol. 14, no. 2, pp. 131–145, 1999.

[10] K.-U. Bletzinger, R. Wüchner, F. Daoud, and N. Camprubí, "Computational methods for form finding and optimization of shells and membranes," *Computer Methods in Applied Mechanics and Engineering*, vol. 194, no. 30-33, pp. 3438–3452, 2005.

[11] F. Dieringer, B. Philipp, R. Wüchner, and K. U. Bletzinger, "Numerical methods for the design and analysis of hybrid structures," *International Journal of Space Structures*, vol. 28, no. 3-4, pp. 149–160, 2013.

[12] A.-K. Goldbach, A. M. Bauer, R. Wüchner, and K.-U. Bletzinger, "CAD-integrated parametric lightweight design with isogeometric B-rep analysis," *Frontiers in Built Environment*, vol. 6, 2020.

[13] Y. Shen, P. D'Acunto, J.-P. Jasienski, and P. O. Ohlbrock, "A new tool for the conceptual design of structures in equilibrium based on graphic statics," *International fib Symposium - Conceptual Design of Structures 2021*, 2021.

[14] P. D'Acunto, J.-P. Jasienski, P. O. Ohlbrock, C. Fivet, J. Schwartz, and D. Zastavni, "Vector-based 3D graphic statics: a framework for the design of spatial structures based on the relation between form and forces," *International Journal of Solids and Structures*, vol. 167, pp. 58–70, 2019.

[15] M. Konstantatou, P. D'Acunto, and A. McRobie, "Polarities in structural analysis and design: N-dimensional graphic statics and structural transformations," *International Journal of Solids and Structures*, vol. 152, pp. 272–293, 2018.

[16] R. Pastrana, P. O. Ohlbrock, T. Oberbichler, P. D'Acunto, and S. Parascho, "Constrained form-finding of tension-compression structures using automatic differentiation," 2021, https://arxiv.org/abs/2111.02607.

[17] A. M. Widhammer, *Variation of Reference Strategy. Generation of Optimized Cutting Patterns for Textile Fabrics*, Dissertation at Technische Universität München, Munich, Germany, 2015.

[18] K.-U. Bletzinger and A. M. Widhammer, "Variation of reference strategy - a novel approach for generating optimized cutting patterns of membrane structures," *Procedia Engineering*, vol. 155, pp. 131–141, 2016.

[19] B. Maurin and R. Motro, "Cutting pattern of fabric membranes with the stress composition method," *International Journal of Space Structures*, vol. 14, no. 2, pp. 121–129, 1999.

[20] F. Dieringer, *Numerical Methods for the Design and Analysis of Tensile Structures*Dissertation at Technische Universität München, Munich, Germany, 2014.

[21] A.-K. Goldbach, M. Breitenberger, A. M. Widhammer, and K.-U. Bletzinger, "Computational cutting pattern generation using isogeometric B-rep analysis," *Procedia Engineering*, vol. 155, pp. 249–255, 2016.

[22] S. Govindjee and P. A. Mihalic, "Computational methods for inverse finite elastostatics," *Computer Methods in Applied Mechanics and Engineering*, vol. 136, no. 1-2, pp. 47–57, 1996.

[23] S. Govindjee and P. A. Mihalic, "Computational methods for inverse deformations in quasi-incompressible finite elasticity," *International Journal for Numerical Methods in Engineering*, vol. 43, no. 5, pp. 821–838, 1998.

[24] Y. Q. Guo, J. L. Batoz, J. M. Detraux, and P. Duroux, "Finite element procedures for strain estimations of sheet metal forming parts," *International Journal for Numerical Methods in Engineering*, vol. 30, no. 8, pp. 1385–1401, 1990.

[25] J. M. F. Linhard, *Numerisch-Mechanische Betrachtung des Entwurfsprozesses von Membrantragwerken [Numerical Mechanical Analysis of the Design Process of Membrane Structures] [German]*, Dissertation at Technische Universität München, Munich, Germany, 2009.

[26] J. M. F. Linhard, R. Wüchner, and K.-U. Bletzinger, "Introducing cutting patterns in form finding and structural analysis," *Textile Composites and Inflatable Structures II*, vol. 8, pp. 69–84, 2008.

[27] K.-U. Bletzinger, J. M. F. Linhard, and R. Wüchner, "Extended and integrated numerical form finding and patterning of membrane structures," *Journal of the International Association for Shell and Spatial Structures*, vol. 50, 2009.

[28] K. B. Sautter, "github," 2022, https://github.com/KlausBSautter/Find_Reference_Truss_3D.

[29] K. B. Sautter, M. Meßmer, T. Teschemacher, and K.-U. Bletzinger, "Limitations of the St. Venant–Kirchhoff material model in large strain regimes," *International Journal of Non-linear Mechanics*, vol. 147, Article ID 104207, 2022.

[30] A. S. Ramos and G. H. Paulino, "Convex topology optimization for hyperelastic trusses based on the ground-structure approach," *Structural and Multidisciplinary Optimization*, vol. 51, no. 2, pp. 287–304, 2014.

[31] T. Belytschko, W. K. Liu, B. Moran, and K. Elkhodary, *Nonlinear Finite Elements for Continua and Structures*, p. 978, John Wiley & Sons, New Jersey, NJ, USA, 2014.

[32] P. Dadvand, R. Rossi, and E. Oñate, "An object-oriented environment for developing finite element codes for multidisciplinary applications," *Archives of Computational Methods in Engineering*, vol. 17, no. 3, pp. 253–297, 2010.

[33] P. Dadvand, R. Rossi, M. Gil et al., "Migration of a generic multi-physics framework to HPC environments," *Computers & Fluids*, vol. 80, pp. 301–309, 2013.

[34] Kratos, "GitHub repository," 2022, https://github.com/KratosMultiphysics/Kratos.